Cross-layer Analysis of Optimal Relaying Strategies for Terahertz-band Communication Networks

Qing Xia and Josep Miquel Jornet

Department of Electrical Engineering
University at Buffalo, The State University of New York
Buffalo, New York 14260, USA
E-mail: {qingxia, jmjornet}@buffalo.edu

***Abstract*— Terahertz (THz) band (0.1-10 THz) communication, which is envisioned as one of the key wireless communication technologies of the next decade, exhibits an extremely large bandwidth at the cost of an extremely high path loss. The unique distance-dependent behavior on the available bandwidth in THz communication interrelates all THz properties, and affects the design and performances within and across the physical, link and network layers. More specifically, the limited transmission power, combined with the high path loss, requires the use of directional antennas (DAs). High DAs have a clear impact at the link layer as well as the network layer, where relaying becomes a requirement. In this paper, optimal relaying strategies for THz-band communication networks are investigated. More specifically, a mathematical framework is formulated and used to study the optimal relaying distance that maximizes the network throughput by taking into account the cross-layer effects between the channel, the antenna, and the physical, link and network layers. Numerical results are provided to illustrate the importance of accurate cross-layer design strategies for THz networks.**

***Keywords*—THz band communication, cross-layer design, optimal relaying strategies, directional antennas.**

1. Introduction

Over the last decade, wireless data traffic has significantly increased because of the way today's society creates, shares and consumes information. A growing demand for higher speed wireless communication substantially stimulate this change. For instance, wireless data rates have doubled every eighteen months over the last three decades and are quickly reaching the capacity of wired communication systems. Following the trend of drastically increased data traffic, wireless Terabit-per-second (Tbps) links are expected to become a reality in the close future, saying, next five to ten years. Terahertz (THz)-band (0.1-10 THz) communication is envisioned as a key technology to satisfy the need for such very high data-rates [1].

For many years, the lack of compact and efficient approaches to generate and detect THz-band signals has limited the achievability of THz-band communication systems. However, within the last several years, outstanding progress has been achieved towards the development of compact THz-band transceivers and antennas. Different technologies has been considered to date, ranging from Silicon Germanium [2] and compound semiconductor technologies based on III-V semiconductors [3], to photonics devices such as Quantum Cascade Lasers (QCLs) [4] and, more recently, plasmonic devices based on novel materials such as graphene and other 2D nanomaterials [5].

The THz-band provides wireless communication THz devices with an unprecedentedly large bandwidth (several tens of GHz to a few THz) [6], [7]. The main phenomenon affecting the propagation of THz-band signals is the absorption by water vapor molecules. For communication distances beyond a few meters, molecular absorption defines multiple transmission windows, each of them tens or hundreds of GHz wide. In this cases, physical-layer data-rates in the order of hundreds of Gigabit-per-second (Gbps) and few Tbps have already been demonstrated, even with low-complexity modulations [8].

In parallel to the development of THz-devices and physical layer mechanisms, there is a need to investigate new network solutions for very-high-speed wireless data networks. In [9], an Assisted Beamforming Medium Access Control (MAC) protocol for THz-band communication networks was presented. This protocol relies on the 2.4 GHz channel to synchronize the transmitter and the receiver and schedule the data transmission through the THz channel using beamforming. The THz MAC protocol in [10] relies on the use of high-speed turning DAs to overcome high path-loss at THz-band frequencies and establish links beyond one meter. The protocol guarantees tight synchronization between transmitter and receiver by relying on a receiver-initiated handshake and the steering system control of DAs.

The need of highly DAs simultaneously in transmision and reception introduces further challenges as we move up in the protocol stack [1]. Prior to routing, one of the key questions to answer relates to the optimal relaying distance in multi-hop communication links. Due to the unique distance-dependent behavior of the available bandwidth, the reduction of the transmission distance results in a twofold benefit. On the one hand, as in any wireless communication

978-1-5386-3839-2/17/$31.00 ©2017 IEEE
Authorized licensed use limited to: Northeastern University. Downloaded on January 24,2023 at 04:05:06 UTC from IEEE Xplore. Restrictions apply.

system, for a fixed transmission power, the SNR increases and higher order modulation can be utilized to increase the actual data rate. On the other hand, because of the behavior of molecular absorption in THz frequencies, shorter distances also benefit from a substantially larger transmission bandwidth, which again contributes to the increase of achievable data-rates. However, the need for more hops to cover the same distance and the computational cost of relaying data at multi-Gbps or even Tbps pose a constraint on the system design. As a result, there is an optimal number of relays or, equivalently, an optimal relaying distance.

In this paper, we investigate optimal relaying strategies for THz-band communication networks. More specifically, based on the unique distance-dependent bandwidth property of THz-band communication networks, we formulate a mathematical framework to derive the optimal relaying distance that maximizes the network throughput by taking into account the cross-layer effects between the channel, the antenna and the physical, link and network layers. We also provide numerical results to illustrate the performance of the proposed relaying strategies and the importance of cross-layer design strategies for THz networks.

The rest of the paper is organized as follows. We summarize the related work in Sec. 2. In Sec. 3, we describe the system model, including network topology and operation, channel and DA models, and MAC and neighbor discovery protocol models with DAs. Then, in Sec. 4, a directivity-sensitive buffer and queueing system model are developed, based on which, the analysis of the directional queueing system is formulated. The simulation results is provided in Sec. 5. We conclude in Sec. 6.

2. Related Work

Existing multi-hop relaying strategies designed for lower frequencies cannot be directly applied in the THz band, since they do not capture the aforementioned peculiarities of the THz band. For example, in [11], the authors chose the relays by optimally allocating the energy and bandwidth resources based on the available channel state information, this design is proposed for the resource constrained networks. In [12], the authors incorporated both user traffic demands and the physical channel realizations in a cross layer design to select the best relay, the approach is designed for a cellular system operating in a frequency-selective slow-fading environment.

To the best of our knowledge, a cross-layer study of the optimal relaying distance at THz frequencies has not been conducted before. Millimeter-wave (mmWave) technology (30 to 300 GHz), is the closest existing technology. Several similarities are shared between THz-band communication and mmWave-band communication. For instance, both technologies are designed for high data rate (up to multi-Tbps and multi-hundred-Gbps respectively) communication, also, both technologies suffer tremendous path loss, and, thus, require very high directivity antennas to overcome this limitation. However, there are several differences between mmWave and THz-band communication networks, which arise from the fact that at THz frequencies DAs are simultaneously needed in transmission and reception to complete any meaningful data transaction.

In [13] and [14], the authors mainly considered the cross layer design from physical layer characteristics to MAC layer protocols, network layer performance was not considered. The authors in [15] considered cross layer design from PHY until multi-hop MAC, however, they assumed that multiple short hops can attain higher throughput without considering the increased queueing delay following by this assumption. In [16], the authors introduced a cross-layer model to determine network link connectivity as a function of the locations of relays, the approach take into accounts for two unique peculiarities of mmWave including interference and blockage, which, as introduced before, weakened in the THz-band communication network.

3. System Model

In this section, we firstly provide a brief introduction of the network scenario. Then, we introduce the highly DAs, which are considered to overcome extremely high path loss in THz-band communication networks. We express the DAs' characteristics, such as antenna gain and antenna beam width, as functions of the transmission distance, which affects the performance of multi-hop queueing system in the network layer. In the end of this section, we include the design of neighbor discovery with highly DAs for the reason that the highly DAs brought us new issues when it comes to the network layer design regarding the process of neighbor discovery.

3.1. Network Topology and Operation

We consider that all the nodes are randomly distributed in a flat area following a spatial Poisson distribution. Each node periodically switches between transmission (TX) mode and receiving (RX) mode. A node in TX mode, i.e., with data to transmit, checks whether a Clear-To-Send (CTS) frame from the intended receiver has been recently received. We consider that a CTS frame is valid for duration of facing time. The transmitter who has data to send to a receiver, can only proceed with DATA frame transmission after receiving a valid CTS frame from that receiver, otherwise, the transmitter listens to the channel until the reception of a new CTS frame. A node in RX mode periodically broadcasts its status by CTS frame. We showed in [10] that such receiver-initiated MAC outperforms more conventional transmitter-initiated protocols when the channel bandwidth is not a constraint, but synchronization between devices is.

A fixed number of nodes operate as relays, who, on the one hand, help to relay other nodes' packets, and on the other hand, also generate their own packets. As opposed to relays, the rest of nodes will never relay other nodes' packets. The network is formed as an ad-hoc architecture, whose coverage range can be extended with the help of the relays. As shown in Fig. 1, the relays are marked as black nodes, and are uniformly distributed in the whole network

Authorized licensed use limited to: Northeastern University. Downloaded on January 24,2023 at 04:05:06 UTC from IEEE Xplore. Restrictions apply.

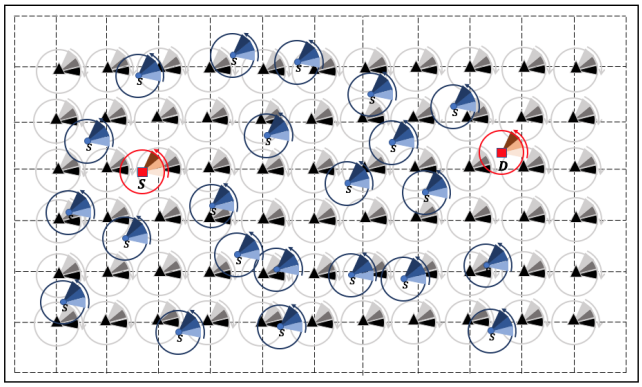

Figure 1: Network Architecture

to guarantee the network connection of any node from any direction. The rest nodes are marked as blue nodes, within which we picked two as the source and the destination for our multi-hop end-to-end (E2E) link analysis and are colored in red. The goal of this paper is to determine the optimal relay transmission range for such a network with multi-hop E2E links.

3.2. Channel and DA Models

The unique distance-dependent characteristic of THz communication is caused by the physics of the channel. The propagation of electromagnetic waves at THz-band frequencies is mainly affected by molecular absorption, which is transmission distance dependent and frequency selective [18]. We consider that transmitters operate at the first absorption defined window above 1 THz. The 3 dB window bandwidth varies with the distance d_T, i.e., longer transmission distance results in a narrower 3 dB bandwidth window, see Fig. 2.

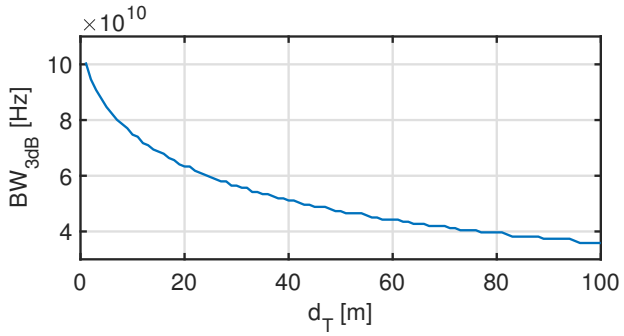

Figure 2: 3 dB bandwidth as a function of transmission range

Molecular absorption results in both molecular absorption loss and molecular absorption noise, both of which, are transmission distance dependent parameters. In particular, based on the THz-band channel model introduced in [6], the signal power at a transmission distance d_T from the transmitter, P_r is given by

$$P_r\left(d_T\right)=\int_{B(d_T)} S_t\left(f\right)\left|H_c\left(f,d_T\right)\right|^2 G_t\left(d_T\right) G_r\left(d_T\right) df, \tag{1}$$

where $S_t(f)$ is the single-sided power spectral density (p.s.d) of the transmitted signal, $B(d_T)$ stands for the 3 dB bandwidth in respect of different transmission range. f refers to frequency and $H_c(f, d_T)$ refers to the THz-band channel frequency response, which is given by

$$H_c\left(f,d_T\right)=\left(\frac{c}{4\pi f d_T}\right)\exp\left(-\frac{k_{abs}\left(f\right)d_T}{2}\right), \tag{2}$$

where c refers to the speed of light and $k_{abs}(f)$ is the molecular absorption coefficient of the medium. This parameter depends on the molecular composition of the transmission medium, i.e., the type and concentration of molecules found in the channel and is computed as in [6]. $G_t(d_T)$ and $G_r(d_T)$ refer to the gain of transmitter antenna and receiver antenna respectively, which are transmission distance dependent parameters.

Similarly, the molecular absorption noise power $N_r(d_T)$ at a distance d_T from the transmitter, which can be modeled as additive, Gaussian, colored and correlated to the transmitted signal [8], is given by

$$N_r\left(d_T\right)=\int_{B(d_T)}\left(S_{N^B}\left(f\right)+S_{N^I}\left(f,d_T\right)\right)\left|H_r\left(f\right)\right|^2 df, \tag{3}$$

where it is taken into account that the total molecular absorption noise is contributed by the background atmospheric noise p.s.d., S_{N^B} and the self-induced noise p.s.d., S_{N^I}, and are computed as described in [8].

To overcome the very high molecular absorption loss over long distances and increase the signal to noise ratio (SNR), highly DAs are applied to both transmitters and receivers with gains as $G_t(d_T)$ and $G_r(d_T)$. Thus, an accurate set of antenna parameters need to be calculated by satisfying the condition that the received signal strength should surpass the received signal power threshold, i.e.,

$$\int_{B(d_T)} S_t\left(f\right)\frac{c^2}{\left(4\pi d_T f\right)^2}e^{-k_{abs}(f)d_T}G_t\left(d_T\right)G_r\left(d_T\right)df \geq N_r\left(d_T\right)SNR_{min}, \tag{4}$$

where SNR_{min} stands for the minimum SNR threshold (10 dB in our analysis). In order to guarantee the performance of highly directive antennas achieved by beam forming antenna arrays, we derive the required antenna gain and resulting antenna beam width from the transmission distance, transmitted signal power and the SNR_{min} threshold. Without loss of generality, the antenna gains of the transmitter and the receiver are considered as identical and constant over the 3 dB frequency window, i.e., $G_t(d_T) = G_r(d_T) = G(d_T)$. In this case, the desired antenna gain can be expressed as:

$$G(d_T)\geq\sqrt{\frac{N_r\left(d_T\right)SNR_{min}}{\int_{B(d_T)} S_t\left(f\right)\frac{c^2}{\left(4\pi d_T f\right)^2}e^{-k_{abs}(f)d_T}df}}. \tag{5}$$

Authorized licensed use limited to: Northeastern University. Downloaded on January 24,2023 at 04:05:06 UTC from IEEE Xplore. Restrictions apply.

We consider that the beamforming antenna array at each regular node is a nearly broadside planar array [19], the directivity of the DA can be approximated as:

$$D(d_T) = \frac{4\pi}{\Omega_A(d_T)} = \frac{4\pi}{\theta_h(d_T)\phi_h(d_T)} \geq G(d_T), \quad (6)$$

where $\Omega_A(d_T)$ refers to the array solid beam angle, $\theta_h(d_T)$ and $\phi_h(d_T)$ are the Half Power Beam Width (HPBW) in the elevation plane and azimuthal plane, respectively. If we assume the HPBW in the elevation plane and azimuthal plane are identical, i.e., $\theta_h(d_T) = \phi_h(d_T) = \Delta\theta(d_T)$, the beam width of the DA can be calculated as follows:

$$\Delta\theta(d_T) \leq \sqrt{4\pi\sqrt{\frac{\int_{B(d_T)} S_t(f)\,\frac{c^2}{(4\pi d_T f)^2} e^{-k_{abs}(f)d_T}\,df}{N_r(d_T)\,SNR_{min}}}}. \quad (7)$$

3.3. Neighbor Discovery with DAs

We consider that the deafness problem is partially overcome by utilizing high-speed turning DAs, as we recently proposed in [10]. The turning speed of DAs is designed to guarantee at least a complete transmission process during one sector time of DAs. As we introduced in Sec. 3.1, each node switches between TX mode and RX mode periodically. In order to increase the facing probability, we assume that when a node is in the TX mode, it turns in the clockwise direction. In contrast, when a node is in the RX mode, it turns in the counter clockwise direction. However, as illustrated in Fig. 3, the opposite turning directions of transmitter and receiver do not necessarily guarantee that they will face each other. The angle difference between transmitter and receiver plays an important role in the facing problem as well. When turning at same speed in opposite directions, the transmitter and receiver will only meet under the condition that their initial angle difference is π.

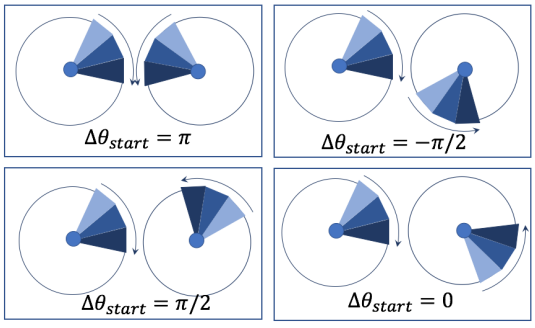

Figure 3: Facing Possibility

In light of this observation, we further specify that the turning speed of transmitter and receiver must be different, thus, the angle difference between transmitter and receiver will change toward a trend of higher possibility of facing if they fail to face in current turning circle. The time duration t for the transmitter and receiver to face each other is calculated by satisfying:

$$\left\| \frac{(\theta_{tx}^{start} + \omega_{tx}t)}{2\pi} \right\| + \pi = \left\| \frac{(\theta_{rx}^{start} - \omega_{rx}t)}{2\pi} \right\|, \quad (8)$$

where θ_{tx}^{start} and θ_{rx}^{start} represent the initial angle of transmitter and receiver respectively, with turning speed of ω_{tx} and ω_{rx}, and $\|\|$ is the modulus symbol.

Besides facing, mode matching is another requirement for communication between transmitter and receiver. To avoid the worst scenario that two neighbors always have exactly the same TX/RX modes distribution in time, we need to shift the nodes' time schedule from each other. One approach is to randomly setup each node at the starting stage of the network, another one is to switch the node's mode from TX mode to RX mode once there is no package stored in its buffer. The detail neighbor discovery protocol will not involved in this paper.

4. Cross-layer Analysis of Relaying Strategies

The highly DAs, as introduced above, help both transmitters and receivers to overcome the tremendous path loss, and thus, extend transmission ranges from several meters to several tens of meters. However, the directional communication property of transceivers highly reduce the relayed packets delivery rate, since the relays will only send out packets after they receives the CTS packet from receiver which could be the next relay or the destination. This is to say, the relay will never remove the first packet from the buffer unless it just received the CTS packet from the direction in which it is facing at and is exactly the destination of its first packet. For this reason, the directivity-sensitive buffer and queueing system will be needed to better arrange the packets flow. In this section, we first design the directivity-sensitive buffer, and then, the corresponding directive-sensitive queueing system, which provide us a more concise and effective way for the further analysis of multi-hop E2E link queueing performance.

4.1. Directivity-sensitive Buffer and Queueing System

As shown in Fig. 4, packets are firstly classified according to their destination's direction when enter the buffer. This process will be achieved once each node collects complete information of its neighbors during previous neighbor discovery process. Then, the classified packets are further passed to sub-buffers in respect of different directions. The number of sub-buffers is the same as the number of sectors within one circle of the directive antenna and is calculated as:

$$N_{sector}(d_T) = \frac{2\pi}{\Delta\theta(d_T)}. \quad (9)$$

The MAC protocol [10] will be embedded in the scheduler which schedules packets exchanges with next relay or destination.

Authorized licensed use limited to: Northeastern University. Downloaded on January 24,2023 at 04:05:06 UTC from IEEE Xplore. Restrictions apply.

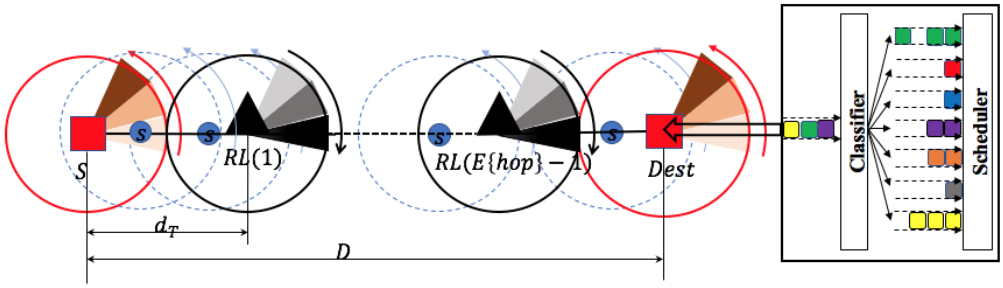

Figure 4: Directivity-sensitive Buffer and Queueing System

With previous design of directivity-sensitive buffer, the relayed packet to different directions will not interfere each other, and in this case, the queueing system can be transferred from previous complex system (as illustrated in Fig. 1), which handle relayed packets from all direction to all direction, to a simpler one that only deals with packets whose destination are in one certain direction (as shown in Fig. 4).

The distance between source and destination is denoted as D, and λ_d refers to the node density on D. Since the nodes location follows poisson distribution, the expected distance between relays on D is calculated as:

$$E\{d\} = \frac{1}{\lambda_d}, \tag{10}$$

thus, $E\{hop\}$, the expected hop number between source and destination on D is:

$$E\{hop\} = \frac{D}{d_T} | d_T \geq E\{d\}. \tag{11}$$

Therefore, $E\{hop\} - 1$ relays participate in the process of relaying packets from source to destination within an E2E link who has totally $E\{hop\}$ hops in between. Besides relaying other nodes' packets, each relay may generate packets to the same direction as well.

To avoid the inefficient queueing delay in the buffer, a sliding window is utilized. All packets in the buffer, consisting of relayed packets and locally generated packets, need to be successfully delivered to the next relay or destination within their facing time. In our analysis, we consider this to be equal to the minimum sector time for one complete transmission:

$$T^{min}_{sector}(d_T) = \frac{N_{packets}(d_T)L_{packets} + N_{control}L_{control}}{R(d_T)} + 2T_{prop}(d_T), \tag{12}$$

where $R(d_T)$ refers to the data-rates in the 3 dB frequency window. $T_{prop}(d_T)$ is the signal propagation delay for a distance of d_T. $L_{packets}$ and $L_{control}$ represents the frame length of the DATA packet and the control packets (e.g., CTS and ACK) respectively. $N_{control}$ is the number of control packets during the process of transmission, two, in our case, since sliding window is applied in our MAC protocol. $N_{packets}(d_T)$ refers to the number of packets need to be delivered to next node within $T^{min}_{sector}(d_T)$, which is:

$$N_{packets}(d_T) = \lambda_g T^{min}_{circle}(d_T) + \lambda_r T^{min}_{sector}(d_T), \tag{13}$$

where λ_g and λ_r stand for local packet generation rate and relayed packet generation rate respectively, and they interrelate each other as:

$$\lambda_r = E\{hop\}\lambda_g. \tag{14}$$

Knowing the number of sectors within one circle, which is given by (9), the minimum circle time can be calculated as:

$$T^{min}_{circle}(d_T) = T^{min}_{sector}(d_T)N_{sector}(d_T). \tag{15}$$

By inserting (13), (14) and (15) back to (12), and arranging $T^{min}_{sector}(d_T)$ to one side, the equation can be simplified as:

$$T^{min}_{sector}(d_T) = \frac{2\left(L_{\text{control}} + R(d_T)T_{\text{prop}}(d_T)\right)}{R(d_T) - \lambda_g L_{\text{packets}}\left(E_{\text{hop}}(d_T) + N_{\text{sector}}(d_T)\right)}, \tag{16}$$

which indicates that the denominator of (16) need to be a positive value, and, thus:

$$\lambda_g \leq \frac{R(d_T)}{L_{\text{packets}}\left(E_{\text{hop}}(d_T) + N_{\text{sector}}(d_T)\right)}. \tag{17}$$

4.2. Directive Queueing Model

With previous cross layer analysis, we illustrated the performance of each directivity-sensitive relay in respect of the unique distance-dependent property. In this section, we will introduce the directivity-sensitive E2E link's performance based on the multi-hop analysis.

For the reason that the transmission of the sliding window will only start by receiving the CTS from the receiver and that there will always have sufficient transmission time with our design, it will be almost impossible to fail during transmission. The interference, unlike that in the mmWave, is much smaller by considering the much narrower beam width for both transmitter and receiver. The blockage will no longer be a issue of failure, since the very fast data-rates in THz-band communication networks results in a scenario that any moving object seems stable. Thus, the Markov chain of our case is shown in Fig. 5, the detail analysis will be illustrated in APPENDIX A.

Authorized licensed use limited to: Northeastern University. Downloaded on January 24,2023 at 04:05:06 UTC from IEEE Xplore. Restrictions apply.

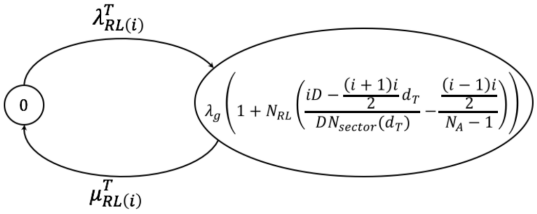

Figure 5: Markov chain representation of the system

The generator matrix is:

$$\boldsymbol{Q}=\begin{bmatrix}-\lambda^T_{RL(i)} & \lambda^T_{RL(i)}\\ \mu^T_{RL(i)} & -\mu^T_{RL(i)}\end{bmatrix}, \tag{18}$$

where $\lambda^T_{RL(i)}$ refers to the total arrival rate of the i^{th} relay which is marked as $RL(i)$ and $\mu^T_{RL(i)}$ is the total departure rate of $RL(i)$. The probability vector can be calculated as:

$$\boldsymbol{\pi}=\begin{bmatrix}\pi_0 & \pi_k\end{bmatrix},$$
$$k=\lambda_g\left(1+N_{RL}\left(\frac{iD-\frac{(i+1)i}{2}d_T}{DN_{sector}(d_T)}-\frac{\frac{(i-1)i}{2}}{N_A-1}\right)\right). \tag{19}$$

Since the steady-state probabilities are independent of time, we have $\mathbf{0}=\boldsymbol{\pi Q}$, which can be extended as:

$$\begin{cases}-\pi_0\lambda^T_{RL(i)}+\pi_k\mu^T_{RL(i)}=0\\ \pi_0\lambda^T_{RL(i)}-\pi_k\mu^T_{RL(i)}=0\end{cases}, \tag{20}$$

giving that $\lambda^T_{RL(i)}=\mu^T_{RL(i)}$, we can solve (20) as $\pi_0=\pi_k=\frac{1}{2}$. We consider the average number of packets in the queueing system is $\overline{K}$, we have:

$$\begin{aligned}\overline{K(d_T)}&=0\pi_0+k\pi_k\\&=\frac{1}{2}\lambda_g\left(1+N_{RL}\left(\frac{iD-\frac{(i+1)i}{2}d_T}{DN_{sector}(d_T)}-\frac{\frac{(i-1)i}{2}}{N_A-1}\right)\right).\end{aligned} \tag{21}$$

Based on the Little's theorem, the average time that a packet spends in the queueing system is denoted as $\overline{T}$ which is calculated as:

$$\overline{T(d_T)}=\frac{\overline{K}}{\lambda^T_{RL(i)}}=\frac{1}{2}T^u, \tag{22}$$

where T^u is the time unite and in our case $T^u=T^{min}_{circle}(d_T)$. Thus, the total queueing delay is:

$$T^{total}_Q(d_T)=\overline{T(d_T)}E\{hop\}=T^{min}_{circle}(d_T)\frac{D}{2d_T}, \tag{23}$$

and the throughput for the packets generated from S to D is calculated as:

$$S_Q(d_T)=\frac{1\times L_{packets}}{T^{total}_Q(d_T)}=\frac{L_{packets}2d_T}{DT^{min}_{sector}(d_T)N_{sector}(d_T)}. \tag{24}$$

For the reason that the transmission distance, as the key parameter, deeply affects the cross-layer properties from the channel, the DA and the physical, link and network layers and interrelates all THz properties. It is extremely complex to form a closed-form solution for the optimal relaying distance, thus, we utilize the numerical analysis to solve this problem.

5. Numerical Results

In this section, unless otherwise stated, we consider a network as introduced above with the following system parameters (Table 1):

TABLE 1: Simulation Parameters

Notation	Parameter	Value
f_c	central frequency	1.0345 [THz]
D	distance between source and destination	100 [m]
SNR_{min}	SNR threshold	10 [dB]

As indicated in Fig. 6, for any fixed generation rate λ_g which satisfies the condition defined in (17), the throughput is a function of transmission range d_T, and there exists an optimal throughput which suggests the preferred transmission range. With an increasing transmission power energy, the throughput will be improved on each d_T, since more packets will be successfully received with much higher SNR than the threshold.

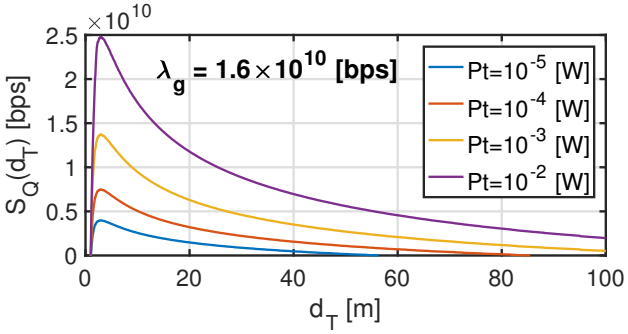

Figure 6: Throughput as a function of transmission range

With an increasing packet generation rate λ_g, the optimal throughput, as shown in Fig. 7, will gradually decrease. Since more sector time need to be scheduled for a larger sliding window containing more DATA packets, meaning that, it will take longer time to face, again, towards the same direction, and the efficiency of a packet transmission will drop correspondingly. Again, higher transmission power energy leads to higher optimal throughput, but it will not change the trend that smaller packets generation rate is always preferred.

The optimal transmission range with respect of the packets generation rate is illustrated in Fig. 8, from which we observe that the optimal transmission range increases with the growing of packets generation rate. This property indicates that less relays are expected in a heavier load system. With the increasing of the transmission power energy, the optimal transmission range will growing correspondingly.

Authorized licensed use limited to: Northeastern University. Downloaded on January 24,2023 at 04:05:06 UTC from IEEE Xplore. Restrictions apply.

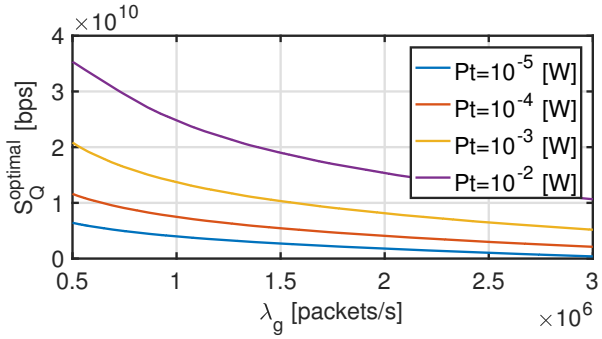

Figure 7: Optimal Throughput

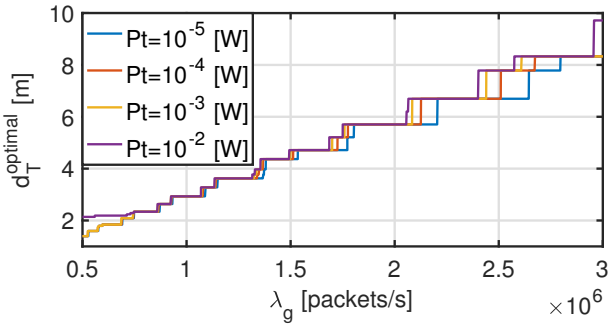

Figure 8: Optimal Transmission Range

6. Conclusion

In this paper, we have explored optimal relaying strategies for THz-band communication networks. Based on the unique distance-dependent behavior of THz-band communication networks, a mathematical framework has been devised and analyzed to derive the optimal relaying distance by taking into consideration the cross-layer affects between the channel, the highly directional antenna and the physical, link and network layers. The optimal relaying performance with respect to several factors such as transmission distance, transmission power energy and packets generation rate has been numerically investigated. The extensive numerical results have been presented to illustrate the importance of the cross-layer design strategies for THz networks.

Acknowledgment

This work was partially supported by the Air Force Office of Scientific Research (AFOSR) under Grant FA9550-16-1-0188.

APPENDIX A

Assume that $RL(x)$ represents the x^{th} relay, $A_{RL}(1)$ refers to one sector coverage area of the $RL(1)$, $N_{RL}(j)$ is the number of nodes in one sector coverage area. $A_{RL}(j-1)+A_{RL}(j)=2A_{RL}$, $A_{RL(0)}=A_S$. The sector coverage area is constant, we have:

$$A_{RL}=\frac{d_T^2}{4}\tan\left(\frac{\Delta\theta(d_T)}{2}\right).$$

Since all nodes are distributed in the whole area following the poisson distribution, the number of nodes containing in each sector coverage area is also constant:

$$\begin{aligned}N_{RL}&=\sum_{i=0}^{N_A} i\frac{(\lambda_A 2A_{RL})^i}{i!}e^{-\lambda_A 2A_{RL}}\\&=\sum_{i=0}^{N_A} i\frac{\left(\lambda_A\frac{d_T^2}{2}\tan\left(\frac{\Delta\theta(d_T)}{2}\right)\right)^i}{i!}e^{-\left(\lambda_A\frac{d_T^2}{2}\tan\left(\frac{\Delta\theta(d_T)}{2}\right)\right)}.\end{aligned}$$

The traffic flow in a E2E link is analyzed as follows: For the first relay $RL(1)$, the arrival packets may, on the one hand, come from source S to the first relay $RL(1)$:

$$\lambda_S^{RL(1)}=\lambda_g,$$

and on the other hand, from other source nodes s to the first relay. As it shown in Fig. 9, for the source node s who's destination is not any of RL or D on the E2E link, the packet of this s would not be put in this sub-queue.

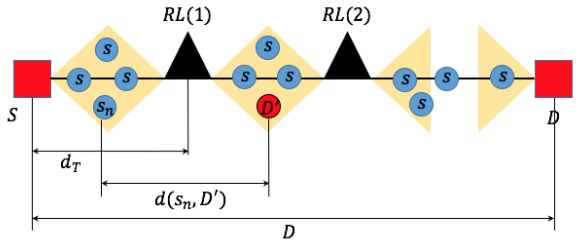

Figure 9: E2E link traffic flow

$$\begin{aligned}\lambda_s^{RL(1)}&=\lambda_g N_{RL}P\left\{\theta(s_n\to D')==\theta(S\to D)\right\}\\&\quad P\{d_T\le d(s_n,D')\le D\}\\&=\lambda_g N_{RL}\frac{1}{N_{sector}(d_T)}\frac{D-d_T}{D}\\&=\lambda_g N_{RL}\frac{D-d_T}{DN_{sector}(d_T)},\end{aligned}$$

where $P\left\{\theta(s_n\to D')==\theta(S\to D)\right\}$ refers to the probability that the destination D' of any other source s_n in $A_{RL}(1)$ aligns the E2E link from S to D, and $P\{d_T\le d(s_n,D')\le D\}$ is the probability that s_n will relay packets to D' by $RL(1)$.

Thus, the total arrival packets to the first relay is $\lambda_{RL(1)}$:

$$\begin{aligned}\lambda_{RL(1)}&=\lambda_S^{RL(1)}+\lambda_s^{RL(1)}\\&=\lambda_g\left(1+N_{RL}\frac{D-d_T}{DN_{sector}(d_T)}\right),\end{aligned}$$

the total delivered packets to the first relay is $\mu_{RL(1)}$:

$$\begin{aligned}\mu_{RL(1)}&=\lambda_g N_{RL(1)}P\{dest=RL(1)\}\\&=\lambda_g N_{RL}\frac{1}{N_A-1}.\end{aligned}$$

Authorized licensed use limited to: Northeastern University. Downloaded on January 24,2023 at 04:05:06 UTC from IEEE Xplore. Restrictions apply.

The number of packets delivered from $RL(1)$ to $RL(2)$ is:

$$\mu_{RL(1)}^{RL(2)} = \lambda_{RL(1)} - \mu_{RL(1)} = \lambda_g \left(1 + N_{RL}\left(\frac{D - d_T}{DN_{sector}(d_T)} - \frac{1}{N_A - 1}\right)\right),$$

on above analysis, we extend the analysis from the first relay to the j^{th} relay:

$$\lambda_{RL(j)}^{RL(j+1)} = \mu_{RL(j)}^{RL(j+1)} = \begin{cases} \lambda_g \left(1 + N_{RL}\left(\frac{D - d_T}{DN_{sector}(d_T)} - \frac{1}{N_A - 1}\right)\right) & \text{if } j = 0 \\ \lambda_g \left(1 + N_{RL}\left(\frac{jD - \frac{(j+1)j}{2} d_T}{DN_{sector}(d_T)} - \frac{\frac{(j+1)j}{2}}{N_A - 1}\right)\right) & \text{if } j > 0 \end{cases}.$$

To summarize, the total arrival rate of the j^{th} relay $\lambda_{RL}(j)^T$ and the total departure rate of the j^{th} relay $\mu_{RL}(j)^T$ can be calculated as:

$$\lambda_{RL(j)}^T = \lambda_{RL(j)},$$

$$\mu_{RL(j)}^T = \mu_{RL(j)}^{RL(j+1)} + \mu_{RL(j)} = \lambda_{RL(j)}.$$

References

[1] I. F. Akyildiz, J. M. Jornet, and C. Han, "Terahertz band: Next frontier for wireless communications," *Physical Communication*, vol. 12, pp. 16–32, 2014.

[2] E. jefors, J. Grzyb, Y. Zhao, B. Heinemann, B. Tillack, and U. R. Pfeiffer, "A 820ghz sige chipset for terahertz active imaging applications," in *2011 IEEE International Solid-State Circuits Conference*, Feb 2011, pp. 224–226.

[3] K. Shinohara, D. C. Regan, Y. Tang, A. L. Corrion, D. F. Brown, J. C. Wong, J. F. Robinson, H. H. Fung, A. Schmitz, T. C. Oh, S. J. Kim, P. S. Chen, R. G. Nagele, A. D. Margomenos, and M. Micovic, "Scaling of gan hemts and schottky diodes for submillimeter-wave mmic applications," *IEEE Transactions on Electron Devices*, vol. 60, no. 10, pp. 2982–2996, Oct 2013.

[4] Q. Y. Lu, N. Bandyopadhyay, S. Slivken, Y. Bai, and M. Razeghi, "Widely tuned room temperature terahertz quantum cascade laser sources based on difference-frequency generation," *Applied Physics Letters*, vol. 101, no. 25, p. 251121, 2012.

[5] J. M. Jornet and I. F. Akyildiz, "Graphene-based plasmonic nano-antenna for terahertz band communication in nanonetworks," *IEEE JSAC, Special Issue on Emerging Technologies for Communications*, vol. 12, no. 12, pp. 685–694, Dec. 2013.

[6] ——, "Channel modeling and capacity analysis of electromagnetic wireless nanonetworks in the terahertz band," *IEEE Transactions on Wireless Communications*, vol. 10, no. 10, pp. 3211–3221, Oct. 2011.

[7] S. Priebe and T. Kurner, "Stochastic modeling of thz indoor radio channels," *IEEE Transactions on Wireless Communications*, vol. 12, no. 9, pp. 4445–4455, 2013.

[8] J. M. Jornet and I. F. Akyildiz, "Femtosecond-long pulse-based modulation for terahertz band communication in nanonetworks," *IEEE Transactions on Communications*, vol. 62, no. 5, pp. 1742 – 1754, May 2014.

[9] X.-W. Yao and J. M. Jornet, "Tab-mac: Assisted beamforming mac protocol for terahertz communication networks," *Nano Communication Networks*, vol. 9, pp. 36 – 42, 2016. [Online]. Available: http://www.sciencedirect.com/science/article/pii/S1878778916300229

[10] Q. Xia, Z. Hossain, M. Medley, and J. M. Jornet, "A link-layer synchronization and medium access control protocol for terahertz-band communication networks," in *2015 IEEE Global Communications Conference (GLOBECOM)*, Dec 2015, pp. 1–7.

[11] Y. w. Hong, W. j. Huang, F. h. Chiu, and C. c. J. Kuo, "Cooperative communications in resource-constrained wireless networks," *IEEE Signal Processing Magazine*, vol. 24, no. 3, pp. 47–57, May 2007.

[12] T. C. y. Ng and W. Yu, "Joint optimization of relay strategies and resource allocations in cooperative cellular networks," *IEEE Journal on Selected Areas in Communications*, vol. 25, no. 2, pp. 328–339, February 2007.

[13] C. S. Sum, Z. Lan, R. Funada, J. Wang, T. Baykas, M. A. Rahman, and H. Harada, "Virtual time-slot allocation scheme for throughput enhancement in a millimeter-wave multi-Gbps WPAN system," *IEEE Journal on Selected Areas in Communications*, vol. 27, no. 8, pp. 1379–1389, 2009.

[14] L. X. Cai, L. Cai, X. Shen, and J. W. Mark, "Rex: A randomized exclusive region based scheduling scheme for mmwave wpans with directional antenna," *IEEE Transactions on Wireless Communications*, vol. 9, no. 1, pp. 113–121, January 2010.

[15] J. Qiao, L. X. Cai, X. S. Shen, and J. W. Mark, "Enabling multi-hop concurrent transmissions in 60 ghz wireless personal area networks," *IEEE Transactions on Wireless Communications*, vol. 10, no. 11, pp. 3824–3833, November 2011.

[16] S. Singh, F. Ziliotto, U. Madhow, E. Belding, and M. Rodwell, "Blockage and directivity in 60 ghz wireless personal area networks: from cross-layer model to multihop mac design," *IEEE Journal on Selected Areas in Communications*, vol. 27, no. 8, pp. 1400–1413, October 2009.

[17] C. Liu, M. Li, I. B. Collings, S. V. Hanly, and P. Whiting, "Design and analysis of transmit beamforming for millimeter wave base station discovery," *IEEE Transactions on Wireless Communications*, vol. 16, no. 2, pp. 797–811, Feb 2017.

[18] J. M. Jornet and I. F. Akyildiz, "Channel modeling and capacity analysis for electromagnetic wireless nanonetworks in the terahertz band," *IEEE Transactions on Wireless Communications*, vol. 10, no. 10, pp. 3211–3221, October 2011.

[19] C. A. Balanis, *Antenna theory: analysis and design*. John Wiley & Sons, 2005.

Authorized licensed use limited to: Northeastern University. Downloaded on January 24,2023 at 04:05:06 UTC from IEEE Xplore. Restrictions apply.